Eur. Phys. J. B **49**, 109–118 (2006)
DOI: 10.1140/epjb/e2006-00019-y

THE EUROPEAN PHYSICAL JOURNAL B

Two-phase flow in porous media: dynamical phase transition

H.A. Knudsen[1,a] and A. Hansen[2,b]

[1] Department of Physics, University of Oslo, PB 1048 Blindern, 0316 Oslo, Norway
[2] Department of Physics, Norwegian University of Science and Technology, NTNU, 7491 Trondheim, Norway

Received 7 February 2005 / Received in final form 2 November 2005
Published online 31 January 2006 –

Abstract. We study numerically the behavior of two-phase flow in porous media via the parameters capillary number and viscosity ratio, under steady-state conditions and various levels of saturation. We construct a phase diagram, where the phases are defined according to whether one or both fluids move. We establish a semi-empirical theory for the location of the phase boundaries. The steady-state conditions are obtained by implementing biperiodic boundary conditions.

PACS. 47.55.Mh Fluid flow through porous media

1 Introduction

The field of two-phase flow in porous media is rich with problems of a complex nature. These involve the study of properties on many different length scales and how to bridge the gap between the scales. Furthermore, it is often possible to distinguish between the study of invasion processes and steady-state properties. The methods used in this field range from a set of experimental techniques, theoretical descriptions on different length scales to several numerical models or methods [1,2].

In the petroleum engineering tradition, the main source of experimental information about flow systems has for decades been displacement experiments on core samples [3]. However, for increased theoretical or fundamental understanding, well controlled laboratory experiments have been the key. In particular, in the eighties, the experiments and simulations by Lenormand et al. led to the development of a phase diagram for drainage, i.e., the displacement of a wetting phase by a nonwetting phase [4,5]. Drainage was classified into the regimes of stable displacement, viscous fingering, and capillary fingering. The regime boundaries depend on two dimensionless numbers, the capillary number Ca and the viscosity ratio M.

Two-phase flow consists of more than pure displacement processes. The complexity of ganglion dynamics and the existence of different regimes of flow of bubbles and blobs have been investigated experimentally by the Payatakes group [6–8]. They used etched glass networks for their studies, varying flow parameters within large ranges. By simultaneous injection of two fluids the experiments examine steady-state properties or close to steady-state properties.

We use a simulator for two-phase flow in porous media that is based on the Washburn equation [9], see Section 2. This line of modeling dates back to the mid eighties to Koplik et al. [10]. The work by the Payatakes group is a continuation of this tradition [11,12]. Most of the work on two-phase flow simulation has been in the actual two-phase regime. That is to say that pure invasion processes such as drainage were simulated until breakthrough of the nonwetting phase. The aforementioned regimes, the phase diagram of drainage are well established and their properties much studied. When it comes to simulations for investigating steady-state properties, the majority of the work involves finding relative permeability curves for a wide range of parameters. Much effort has been put into making simulators that are specific for a given porous medium and fluid system. Further, other simulation techniques exist. On a even more detailed scale than our modeling is the work using lattice Boltzmann methods [13–15].

We wish here to take one step back and take a broader look at these systems. Assuming a porous medium with two phases, one wetting and one nonwetting with respect to the medium, there are three possible states of flow: only the nonwetting phase flows, only the wetting phase flows, or both flow simultaneously. Depending on a large set of parameters, the system will find itself within one of these situations. Changing system parameters within appropriate ranges causes the system to undergo what is called a dynamical phase transition. Using the language of thermodynamics and critical phenomena, we provide in this paper a phase diagram for steady-state flow. As was the case for the phase diagram of Lenormand et al. the capillary number and the viscosity ratio are the parameters

[a] e-mail: h.a.knudsen@fys.uio.no
[b] e-mail: alex.hansen@phys.ntnu.no

of interest also in this primary study of the steady-state phase diagram.

We use a network simulator that can do real steady-state simulations. Phase boundaries are located by the simulations. Further, based on the simulations a semi-empirical theory for the location of the phase boundaries is given. We believe that the overall structure of the phase diagram is universal for the two-phase flow system, whereas the exact positions of phase boundaries will vary from system to system.

2 Model

In order to investigate questions of interest regarding two-phase flow in porous media, it is possible to apply methods that count as theoretical, experimental or numerical. Experimental methods provide quantitative results for the actual system investigated. However, results may differ from sample to sample or from system to system. By means of simulations the system properties can be controlled to a greater extent. This is highly advantageous when one wishes to study the effect of varying parameters of the system.

The results of the paper are based on a network simulator for immiscible two-phase flow. This line of modeling, which is based on the Washburn equation [9], dates back to the work of several groups in the mid 1980's [10–12]. Our model is a continuation of the model developed by Aker et al. [16,17]. Although a thorough presentation can be found in [18], we provide for clarity a brief résumé of the main aspects.

The porous media are represented by networks of tubes, forming square lattices in two dimensions (2D), tilted 45° with respect to the imposed pressure gradient and thus to the overall direction of flow. We refer to the lattice sites where four tubes meet as nodes. Volume in the model is contained in the tubes and the nodes are volumeless joining points. This is just a matter of numerical convenience. Whenever needed, a certain fraction of the volume in the tubes which join in a node can be summed up to an effective node volume. For further details, see [18]. Randomness is incorporated by distorting the nodes randomly within a circle around their respective lattice positions. This gives a distribution of tube lengths in the system. Further, the radii of the tubes are drawn from a flat distribution so that the radius of a given tube is $r \in (0.1l, 0.4l)$, where l is the length of that tube. We note here that this model is perfectly extendable to three dimensions.

The model is filled with two fluid phases that flow within the system of tubes. The flow in each tube obeys the Washburn equation [9], $q = -(\sigma k/\mu)(\Delta p - \sum p_c)/l$. With respect to momentum transfer these tubes are cylindrical with cross-section area σ, length l, and radius r. The permeability is $k = r^2/8$ which is known for Hagen-Poiseuille flow [19]. Further, μ is the viscosity of the phase present in the tube. If both phases are present, the volume average of their viscosities is used. The volumetric flow rate is denoted by q and the pressure difference between the ends of the tube by Δp. The summation is the sum over all capillary pressures p_c within the tube. With respect to capillary pressure the tubes are hour-glass shaped, meaning that a meniscus at position $x \in (0, l)$ in the tube has capillary pressure $p_c = (2\gamma/r)[1-\cos(2\pi x/l)]$, where γ is the interfacial tension between the two phases. This is a modified version of the Young-Laplace law [1,16].

Biperiodic boundary conditions are used so that the flow is by construction steady flow. That is to say, the systems are closed so both phases retain their initial volume fractions, their saturations. These boundary conditions are in 2D equivalent to a flow restrained to be on the surface of a torus. The flow is driven by a globally applied pressure gradient. Usually invasion processes are driven by setting up a pressure difference between two borders, inlet and outlet. Since, by construction, the outlet is directly joined with the inlet in our system, we give instead a so-called global pressure drop when passing a line or cut through the system [18,20]. This is equivalent to imposing constraints on the pressure gradient that is experienced throughout the network. Integration of the pressure gradient along an arbitrary closed path one lap around the system, making sure to pass the 'inlet-outlet'-cut once, should add up to the same global pressure difference.

The system is forward integrated in time using the Euler scheme. For each time step the distribution of the phases leads to a recalculation of the effective viscosities in the tubes and the capillary pressures across the menisci, and thus the coefficients in the equations for the pressure field. When the pressure field is known, the flow field follows automatically and the integration step may be performed. Details are found in [18].

3 Phase diagrams

We present here phase diagrams for the dynamical properties of steady two-phase flow. The structure of the phase diagram is richer than one might naively believe. First we introduce the well-known concept of fractional flow (Eq. (2)) and provide a basic description of the nature of the two-phase flow system. We determine phase boundaries in the parameter space of saturation S_{nw} (defined in Eq. (1)), capillary number Ca (defined in Eq. (4)), and viscosity ratio M (defined in Eq. (3)). The definition of Ca is a crucial point since the definition is not unique. For the numerical exploration of the phase diagram one definition is used consistently in all simulation series: first at constant Ca and varying S_{nw}, second at constant S_{nw} and varying Ca. While Section 3 contains simulated diagrams, Section 4 re-addresses the definition of the capillary number and contains a semi-empirical theory for the location of the phase boundaries that are obtained in Section 3. Upon presenting the method of finding the phase boundaries, the order of the transition is briefly discussed. However, the final discussion of the order is postponed to Section 5.

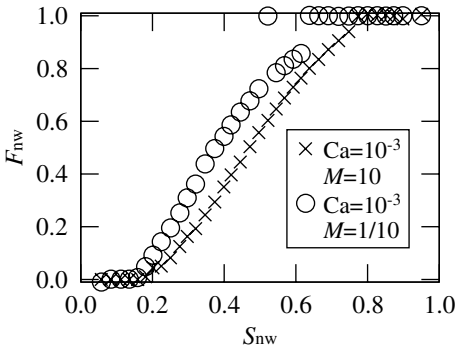

Fig. 1. The nonwetting fractional flow is shown as a function of nonwetting saturation for two sets of system parameters. Each data point is a result of simulation of the model system with the parameters in question until the system reaches steady state and the properties are measured. At low $S_{\rm nw}$ only the wetting phase flows and at high $S_{\rm nw}$ only the nonwetting phase flows. In-between there is a region of two-phase flow. We also observe that the transition of both curves from zero to nonzero $F_{\rm nw}$ is continuous. The transition of $\times$ from two-phase flow to pure nonwetting flow is continuous or weakly first order, while the same transition for $\circ$ is first order. There seems to be a clear jump in the value of $F_{\rm nw}$ as well as indications of hysteresis.

3.1 Order parameter

In steady flow the volume fractions of the wetting and the nonwetting phase will not change with time. In our simulation model this requirement is fulfilled by having a closed system. The nonwetting saturation of the system is defined as

$$S_{\rm nw} = \frac{V_{\rm nw}}{V_{\rm tot}}, \tag{1}$$

where $V_{\rm nw}$ and $V_{\rm tot}$ are the nonwetting and total volume, respectively. The wetting saturation $S_{\rm w}$ is defined similarly. For each value of the saturation, one can in the simulations fix the total flux $Q_{\rm tot}$ in the system. In order to keep the total flux constant, the imposed pressure gradient fluctuates in time around some typical mean value. This mean pressure is a function of saturation and total flux. Further, one can measure the flux of each of the phases in the system, $Q_{\rm nw}$ and $Q_{\rm w}$, respectively. One defines the nonwetting fractional flow as

$$F_{\rm nw} = \frac{Q_{\rm nw}}{Q_{\rm tot}}, \tag{2}$$

and likewise for the wetting fractional flow. A sample of nonwetting fractional flow as a function of nonwetting saturation is given in Figure 1. The transport properties of the system depend on dimensionless groups of system parameters, namely the viscosity ratio and capillary number. We define the viscosity ratio as the nonwetting viscosity divided by the wetting viscosity:

$$M = \frac{\mu_{\rm nw}}{\mu_{\rm w}}. \tag{3}$$

Further, the capillary number is defined as

$$\mathrm{Ca} = \mathrm{Ca}_{\rm dyn} = \frac{Q_{\rm tot}\mu}{\gamma\Sigma}, \tag{4}$$

where γ is the interfacial tension between the two phases, Σ is the cross-section area of the system(i.e. the average diameter of the tubes times the width of the network), and μ is the effective (weighted) viscosity of the system; $\mu = S_{\rm nw}\mu_{\rm nw} + S_{\rm w}\mu_{\rm w}$. Physically, the capillary number measures the ratio between viscous and capillary forces in the system. Use of the weighted viscosity is motivated by the fact that when both phases flow, both viscosities play a role in determining the relative strength of viscous and capillary forces. We use this *dynamical* definition of Ca in this section, upon the exploration of the phase space. For convenience we leave out the subscript of $\mathrm{Ca}_{\rm dyn}$, but we will use it in the subsequent discussion in Section 4 for clarity.

As illustrated in Figure 1 fractional flow curves depend on M and Ca. This dependence is nontrivial. The curves exhibit three different regimes. For low nonwetting saturation only the wetting phase flows. Likewise, for high nonwetting saturation only the nonwetting phase flows. These two regions are thus effectively single-phase flow in a constraining environment consisting of both the solid porous medium and the immobilized phase. In-between these regions is the two-phase flow region. The cross-overs from single-phase flow to two-phase flow are in fact dynamical phase transitions. We wish to study this system with that perspective. As order parameter for the transition from single wetting flow to two-phase flow we use the nonwetting fractional flow. Similarly we take the wetting fractional flow as the order parameter for the transition from single nonwetting flow to two-phase flow. In this way the order parameter is zero for single-phase flow and nonzero for two-phase flow.

Having defined the order parameter, the nature of possible dynamical phase transitions in the system is well illustrated in Figure 1. Starting at the left hand side, the transition is from single-phase wetting flow to two-phase flow when increasing the nonwetting saturation. Both samples show a continuous transition. That is to say that at least to the resolution of the curves the order parameter changes continuously from zero to nonzero values at the phase boundary. The transition of the curve marked with $\circ$ on the right hand side has clear signs of being first order. Not only can we see how the order parameter is discontinuous, but the one isolated data point of $F_{\rm w} = 0.0$ indicates the presence of hysteresis or history dependence in the system. Hysteresis is typical for first order transitions. In fact, we will use studies of hysteresis in order to unravel the nature of the phase diagram. As to the other curve, marked with $\times$, on the right hand side, the transition seems to be continuous or weakly first order.

3.2 Hysteresis loops

In order to map out the phase diagram, we need a tool that can locate the phase boundaries in parameter space. The order of the transitions should also be determined. Simulations of single points in parameter space to steady-state as in Figure 1 are good for the part of parameter

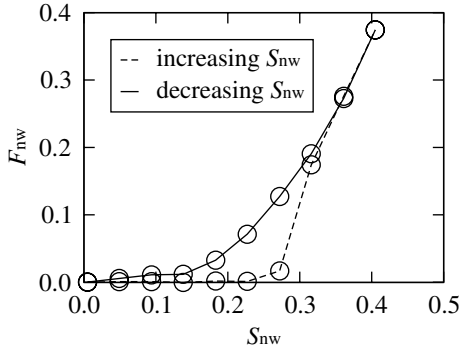

(a) Single-phase wetting flow - two-phase flow.

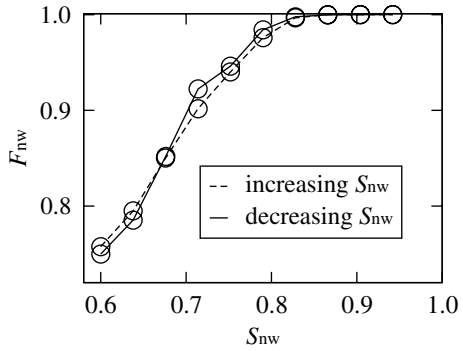

(b) Two-phase flow - single-phase nonwetting flow.

Fig. 2. The stepwise simulation of two phase transitions. In both cases Ca $= 1.00 \times 10^{-3}$ and $M = 10$. The saturation is changed in steps up and down past the transition. The system is run for 7 s (physical time) at each step. (a) Starting at single-phase wetting flow, increasing the saturation above the transition to two-phase flow, and then lowering the saturation back to the initial level, the system shows hysteresis. (b) Starting in the two-phase region and increasing saturation to single-phase nonwetting flow, and decreasing again, no hysteresis appears.

space where history effects are small. However, whenever one is close to a first order transition the history may give data points indicating single-phase flow or two-phase flow. It is possible to run simulations on several statistically equal realizations of the porous media, as well as from various initial configurations, in order to find the region where both single-phase and two-phase flow are possible. The computations are somewhat computer demanding, and we have found it more efficient to simulate entire hysteresis loops to this effect. For instance starting at a specified saturation, at which the system has two-phase flow, we change in a stepwise fashion the saturation slightly, run until steady-state, and measure the fractional flow. This is done until the system passes the transition to single-phase flow. Thereafter the saturation is changed the opposite way until the cross-over from single-phase flow to two-phase flow occurs. In case of a continuous transition, these two points of transition will be the same. However, in case of a first order transition these points will not be the same, and the fractional flow will appear as a hysteresis loop, see Figure 2a.

It is also possible to keep the saturation constant and vary some other parameter, typically the capillary number. Similar loops are expected at first order transitions by this procedure. The advantage of changing Ca is that one simply has to change the total flux Q_{tot} in the system. This is a unique operation, while changing the saturation smoothly is not unique. It requires that one make a choice as to where in the system the changes should be made. In general, we increase or decrease existing bubbles by moving the menisci that define their surface. If the system is very fragmented, some smaller bubbles are typically also removed in order to reach the desired new saturation.

3.3 Diagrams for constant Ca

In this subsection we study one sample of the porous network of size 20×40. We do not yet go into the possible dependence on size and topology, but focus on how the results depend on the three parameters: phase saturation, capillary number Ca, and viscosity ratio M. First we keep Ca and M constant while we vary the saturation stepwise over the transition from single-phase flow to two-phase flow and back.

Examples of transitions between single-phase and two-phase flow are shown in Figure 2. By varying the saturation both ways over the transition, we observe how there can (a), and cannot (b), be hysteresis in the transition. Having a transition with little or without hysteresis as in Figure 2b, leads to a quite precise determination of the transition point. On the other hand it is not so clear where the transition occurs for the sample in Figure 2a. Not only are there two actual transition points, but these two points should be expected to depend on the actual path in parameter space. By that we mean in this case how many steps there are in saturation, and for what time the system is allowed to relax at each step. Further, the variation from sample to sample, or from realization to realization, of systems that are in principle similar, may very well be larger when there is hysteresis of this kind. For curves as in Figure 2b, the statistical variations are smaller. The transitions in Figure 2 were taken to be at (a) $S_{\mathrm{nw}} = 0.26$ and (b) $S_{\mathrm{nw}} = 0.84$. Here we employed that convention that the system is single-phase whenever it is single-phase in one of the simulated directions. This definition is mainly motivated by the need of consistency in the extraction of data points in the following. This is in contrast to the more conventional definition, where the transition is located at the steepest point of the order parameter curve. However, this definition leads to too much noise in the analysis.

The range of capillary numbers studied is Ca $\in (3.16 \times 10^{-2}, 3.16 \times 10^{-4})$. On a base 10 logarithmic scale 9 values of Ca are chosen in steps of 0.25 from -1.50 to -3.50. Similarly 21 values of M are chosen in steps of 0.25 in the interval $\log_{10} M \in (-2.50, 2.50)$, which means that $M \in (-3.16 \times 10^{-3}, 3.16 \times 10^{2})$.

For six of these Ca values, the resulting phase boundaries are shown in Figure 3 as data points. The solid lines are constructed phase boundaries following from

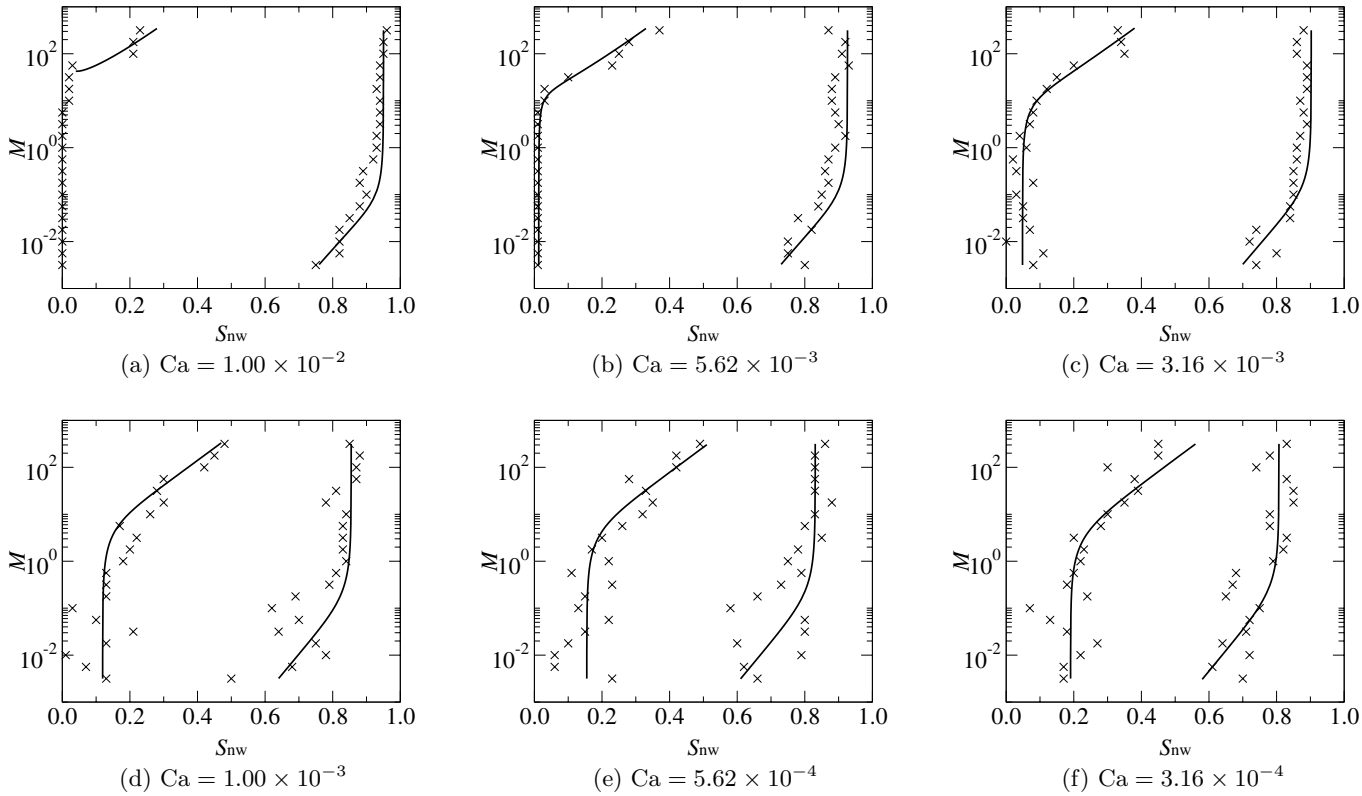

Fig. 3. The phase diagram for six selected values of Ca. The ×-marks are the transition points from the simulations. The uncertainty in each point is not marked, but it is substantial. The scattering of points in parameter space gives an indication of the uncertainty. Phase boundaries are indicated by solid lines, see Section 4. The phase diagrams are divided into three regions, counting from the left hand side: single-phase wetting flow, two-phase flow, and single-phase nonwetting flow.

the semi-empirical theory given in Section 4. For now, let us consider the lines as visual aids to better see the phase boundaries in the diagrams. With increasing nonwetting saturation, the two lines separate the dynamical phases: single-phase wetting flow, two-phase flow, and single-phase nonwetting flow. Observe that for high capillary numbers the two-phase region spans almost all of the saturation range. As the capillary number is lowered, the single-phase regions grow in size. There is some kind of symmetry between the two transitions. That is to say the same effects occur on both sides, although not at the same numerical values.

In order to treat the two transitions simultaneously, we employ the following notions. Since at each transition there is more volume of the phase that is close to single-phase flow, we refer to this phase as the majority phase. The other phase is the minority phase. On the left side the majority phase is wetting and the minority phase is nonwetting. Regarding viscosity ratios M there are basically three possibilities: viscosity matching phases, favorable viscosity ratio, and unfavorable viscosity ratio. Considering the system from the point of view of the majority phase, the viscosity ratio is favorable when the majority phase is the less viscous phase. Likewise, the viscosity ratio is unfavorable when the minority phase is less viscous. On the y-axes of Figure 3 M varies over more than four decades. The positive side (on the logarithmic scale) is when the nonwetting phase is more viscous than the wetting phase. Thus, the viscosity ratio is favorable on the left side and unfavorable on the right side. For negative values of $\log_{10}(M)$ the ratio is unfavorable on the left side and favorable on the right side.

The general structure of the phase diagrams in Figure 3 is as follows. Firstly, for $M = 1$ and high capillary numbers the two-phase region spans almost all of the saturation range. As Ca is lowered the single-phase regions on each side open up, and the two-phase region becomes smaller. We cannot tell from the presented diagrams the limiting behavior of the phase boundaries for small Ca. However, roughly speaking, one observes that the dependence on Ca is logarithmic (also cf. Fig. 4). It is reasonable to expect that this behavior persists also for lower Ca.

The dependence on M is interesting. For all values of Ca the fact that each curve has two main parts persists. Roughly, there is one situation for favorable viscosity ratios and another for unfavorable viscosity ratios. The subsequent discussion of these two situations are made from the two-phase flow point of view. The single-phase point of view is taken in Section 4.

For unfavorable viscosity ratio (lower left and upper right sides in each of the diagrams in Fig. 3) the phase boundaries are almost constant with respect to the value of M. As long as there are clear majority and minority phases, and one phase is close to going single-phase, the

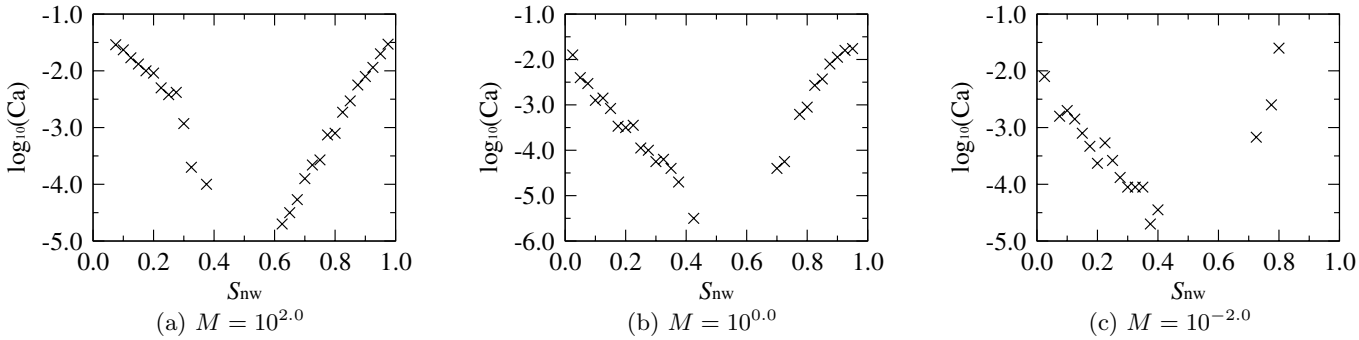

Fig. 4. The phase diagram for three selected values of M. The simulations were performed at constant saturation, but with varying Ca. The simulated points indicate the dynamical phase boundaries. In the lower left part of the diagrams, there is single-phase wetting flow; in the middle upper part, two-phase flow; and in the lower right part, single-phase nonwetting flow.

minority phase consists of bubbles and ganglions that are held back by capillary forces. It is always the case that the minority phase is held back in this way. However, when the viscosity ratio is unfavorable, the minority phase flows more easily, it follows the majority phase around when capillary forces are overcome. Notice that the noise level increases with decreasing Ca. When the capillary forces become relatively stronger, the motion of bubbles involves larger fluctuations, so this behavior is expected when properties are averaged over the same amount of time.

A different situation appears for favorable viscosity ratios. The capillary forces and viscous forces both try to hold back the minority phase. In this situation the actual viscosity ratio plays a role. The more favorable viscosity ratio, the more will the minority phase slow down. Because of the capillary forces the minority phase will not only slow down, but actually stop, and single-phase flow results. The border between two-phase flow and single-phase flow varies with M, as can be seen in Figure 3. We observe the general trend that the single-phase region increases logarithmically with increasingly favorable viscosity ratio.

3.4 Diagrams for constant M

So far we have discussed the results from simulations where the saturation has been varied over the dynamical phase transition. In this subsection we present results from simulations in which the saturation and the viscosity ratio are held constant, while Ca is varied down and up again over the transition. Because of history effects such as hysteresis and the fact that saturation and Ca are not varied in the same way, it is a priori not clear that the phase boundaries will be the same. Therefore, we check the results for consistency.

For nine different values of M, equidistantly distributed on a logarithmic scale between $M = 1/100$ to $M = 100$, simulations have been performed for a large set of saturations. The results for three selected values of M are shown in Figure 4. For large viscosity contrasts it turned out to be difficult to simulate very small saturations of the minority phase, possibly because the transition would occur for very large capillary numbers. More importantly, the central part of the saturation range was also difficult to simulate, because the fluctuations in the systems are larger in this region. One might expect that it is possible for the system to reach either single-phase wetting flow or single-phase nonwetting flow simply as the result of fluctuating into that state. We found that the fluctuations remain large for capillary numbers all the way down to Ca $= 10^{-6}$ for several samples. It is also possible that there is a finite saturation range, where the dynamical phase is two-phase flow for all values of Ca. We conclude that this region therefore may be out of reach with the simulator at hand.

The presented diagrams in Figure 4 have basically the same appearance. They consist of three parts: single-phase wetting flow in the lower left corner, single-phase nonwetting flow in the lower right corner, and two-phase flow in the upper middle region. Secondly, one observes that the phase boundaries may have ending points at zero and unity saturation for finite values of Ca. At higher values of Ca the system has two-phase flow for all saturations. This is expected as high capillary numbers mean vanishing small capillary forces relative to viscous forces.

In order to compare the result from the simulations with constant Ca and constant M, we have plotted all nine data sets for constant M in Figure 5b. In Figure 5a the data for constant Ca have been extracted for the same sets of viscosity ratios as in Figure 5b and plotted using the same axes. In both cases the curves overlap considerably so we have chosen to use the same line style for most of the lines. The exception is that for the three most favorable viscosity ratios of each transition a different line style is used. These three curves separate more and more from the rest of the curves with increasing viscosity contrast. Note that the range of capillary numbers in Figure 5a is smaller than in Figure 5b. The results are not identical, but nevertheless quite close to each other down to Ca $= 10^{-3.5}$. We conclude that the two ways of performing the simulations give consistent results.

A general feature of the diagrams in Figure 5 is that for both the left side boundary and the right side boundary, there seems to be a lower limit. This means that for all viscosity ratios, the respective single-phase region on each

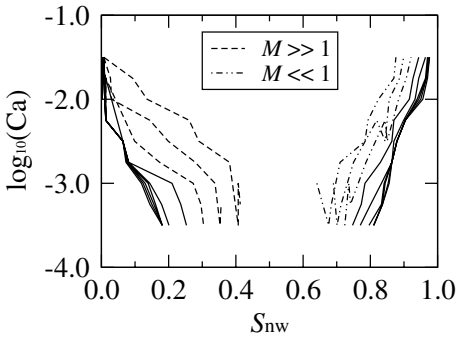

(a) Extracted from constant Ca simulations as shown in Figure 3.

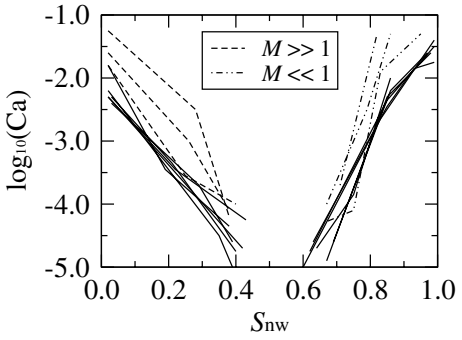

(b) Extracted from constant saturation simulations as shown in Figure 4.

Fig. 5. The phase boundaries from the simulations, of which two subsets are shown in Figures 3 and 4, respectively, are extracted as lines in a $S_{\rm nw} - {\rm Ca}$ coordinate system. Here, M parametrizes the curves and takes the nine values $M = 10^x$ where $x = \{-2.0, -1.5, ..., 2.0\}$.

side extends at least to this limit. Roughly speaking these limits vary logarithmically with Ca. Again we cannot tell if this behavior will continue for lower Ca than depicted.

4 Location of the phase boundaries

In the previous subsection the point of view taken was that of the two-phase flow system. That is to say, we used the dynamical definition of the capillary number, equation (4), and we asked when does one of the phases cease to flow? Reversing the point of view is fruitful. Considering the system starting from a single-phase flow situation, the natural question is when does the second phase start to flow?

Being in a single-phase flow situation, although with both phases present in the system, means that the capillary number should be defined differently. Namely, the relevant viscosity is no longer the volume averaged viscosity, but the viscosity of the fluid that is actually flowing. The wetting and nonwetting capillary number are defined as

$$\mathrm{Ca}_{\rm w} = \frac{Q_{\rm tot}\mu_{\rm w}}{\Sigma\gamma}, \tag{5}$$

and

$$\mathrm{Ca}_{\rm nw} = \frac{Q_{\rm tot}\mu_{\rm nw}}{\Sigma\gamma}, \tag{6}$$

respectively. Here, $\mathrm{Ca}_{\rm w}$ is the relevant capillary number for single-phase wetting flow, whereas $\mathrm{Ca}_{\rm nw}$ is relevant for single-phase nonwetting flow.

As opposed to the qualitative statements regarding the phase boundaries that were made in Section 3, these definitions of the capillary number are also quantitatively useful. For a given system, i.e. given topology and saturation, the transition to two-phase flow takes place at a given wetting (or nonwetting) capillary number. That means with varying value of the viscosity ratio M, which also changes $\mathrm{Ca}_{\rm dyn}$, see equations (4) and (7), the relevant single-phase capillary number still holds a fixed value at the transition. This is plausible as long as the transition to two-phase flow is continuous. In that case the amount of minority phase flowing just after its mobilization is still only a small fraction of the total flow, and therefore the physical effective viscosity is still very close to the viscosity of the single-phase that just before flew alone. However, should the transition be first order so that a finite fraction is mobilized at once, then for large variations in M some corrections should be made. Nevertheless, for now we assume that the single-phase capillary number governs the location of the phase boundaries. The question of the order of the transition is addressed in Section 5, and thereby the validity of this assumption is discussed.

By combining equations (3), (4), and (6), the dynamical capillary number can be written as

$$\begin{aligned}\mathrm{Ca}_{\rm dyn} &= \frac{Q_{\rm tot}\mu_{\rm w}}{\Sigma\gamma}\left(S_{\rm w} + MS_{\rm nw}\right) \\ &= \mathrm{Ca}_{\rm w}S_{\rm w} + \mathrm{Ca}_{\rm w}M(1 - S_{\rm w}),\end{aligned} \tag{7}$$

which is useful to study the transition from single-phase wetting to two-phase flow (left hand side of Fig. 5). Assuming that there exists such a single-phase wetting capillary number that defines the onset of mobilization of the other phase, the corresponding value of the dynamical capillary number is calculated in a straight-forward manner from equation (7). In Figure 5 we observe that there is on the left hand side a limiting line, below which there is always single-phase flow. Since we know that this limit is obtained for $M \ll 1$, we can take the same limit in equation (7) and thereby identify, here on an empirical basis, that the critical wetting capillary number obeys

$$\mathrm{Ca}_{\rm dyn} = \mathrm{Ca}_{\rm w}S_{\rm w} = \mathrm{Ca}_l 10^{-\alpha_l S_{\rm nw}}. \tag{8}$$

The fitted values of Ca_l and α_l are found in the caption of Figure 6. We note here that a similar dependency on Ca was observed in a previous study [21]. There the dependency was shown to be related to percolation theory. It seems plausible that this is also the case here, from which it follows that simple arguments for the behaviour in equation (8) may not exist.

Taking the found value of $\mathrm{Ca}_{\rm w}$ in equation (8) and assuming a given value of $\mathrm{Ca}_{\rm dyn}$, we can solve for M as a

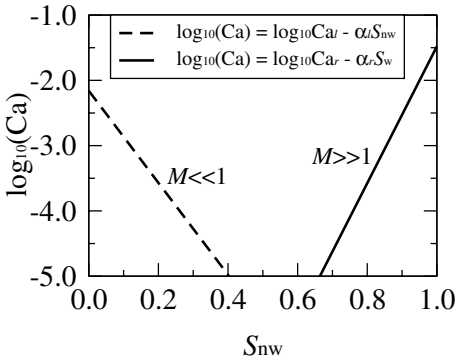

Fig. 6. The phase boundaries in Figure 5 approach a limiting boundary for low M (left side) and large M (right side), and these limits are shown here. The fitted values for the constants are: $\mathrm{Ca}_l = 10^{-2.16}$, $\mathrm{Ca}_r = 10^{-1.48}$, $\alpha_l = 7.04$, and $\alpha_r = 10.42$.

function of S_{nw} and get

$$M = \frac{1 - S_{\mathrm{nw}}}{S_{\mathrm{nw}}} \left(\frac{\mathrm{Ca}_{\mathrm{dyn}} 10^{\alpha_l S_{\mathrm{nw}}}}{\mathrm{Ca}_l} - 1 \right). \tag{9}$$

The interpretation is that (again for a given $\mathrm{Ca}_{\mathrm{dyn}}$) the phase boundary is given by the set of values of M and S_{nw} that fulfill this relationship. This has been done for each of the dynamic capillary numbers in Figure 3 in order to create the solid lines for the left hand side transitions there.

For values of $\mathrm{Ca}_{\mathrm{dyn}} > \mathrm{Ca}_l$, the wetting single-phase region does not exist for all values of M. Still the derived expression works, but the solution only has one branch, as one can see in Figure 3a. That is to say that the single-phase region can only be reached for values of M larger than a certain threshold in this case. This is not the case for $\mathrm{Ca}_{\mathrm{dyn}} < \mathrm{Ca}_l$, where there is a single-phase region for all M.

The boundaries on the right hand side between two-phase flow and single-phase nonwetting flow are found by taking the limit $M \gg 1$ in equation (7), again comparing with the empirical data in the same limit (Fig. 6). The critical nonwetting capillary number is thus found to obey

$$\mathrm{Ca}_{\mathrm{dyn}} = \mathrm{Ca}_{\mathrm{nw}} S_{\mathrm{nw}} = \mathrm{Ca}_r 10^{-\alpha_r S_{\mathrm{w}}}. \tag{10}$$

This result inserted into equation (7) and solved for M gives

$$M = \left[\frac{1 - S_{\mathrm{w}}}{S_{\mathrm{w}}} \left(\frac{\mathrm{Ca}_{\mathrm{dyn}} 10^{\alpha_r S_{\mathrm{w}}}}{\mathrm{Ca}_r} - 1 \right) \right]^{-1} \tag{11}$$

for the phase boundaries in the $\mathrm{Ca}_{\mathrm{dyn}}$-$S$ diagram. By using equation (11) we construct the phase boundaries shown as solid lines on the right hand side in Figure 3. The general good agreement between the simulated data points and these semi-empirical, semi-theoretical lines, serves as a confirmation a posteriori of this theoretical approach. Indeed, we conclude that the single-phase capillary number is the relevant entity that controls the transition to two-phase flow, rather than the more commonly used capillary number defined in equation (4). However, we should point out that from an experimental point of view, it is the conventionally defined capillary number which is the most relevant one.

5 Order of the transitions

So far we have only discussed the location of the dynamical phase boundaries. The order of the transitions across these boundaries should also be discussed. All the simulations presented so far were done on a single system size, namely 20×40 nodes. The main feature that distinguishes between first and second order transition is the existence of a divergent correlation length in the latter. However, the identification of such a correlation length would necessitate a full finite size scaling analysis, which is prohibitively expensive when mapping a large phase space. We therefore use the less reliable but still indicative method of determining whether there is a hysteresis or not.

Each simulation in Figure 3 can be categorized into showing or not showing hysteresis. We look for the general trend while accepting that fluctuations and randomness play a role. Some realizations do not show hysteresis even though all neighboring points do, and vice versa. It turns out that the phase boundaries of Figure 3 can be divided into two logical parts. The almost vertical line segments where the systems have unfavorable viscosity ratio differ from the other parts of the curves where the viscosity ratio is favorable. In the vertical parts the simulations show no or little signs of hysteresis in the order parameter. This indicates that the transitions in these regions are continuous. The fact that the curves are noisy for lower Ca in these regions, does not affect the order. In the sloping parts of the boundaries the order parameter exhibit discontinuity and hysteresis in most simulations. The level of hysteresis increase with increasing viscosity contrast. Hence, this indicates that the transitions in these regions are first order.

In general, it is possible that the appearance of different orders of the transitions is a result of finite size effects, when the determination is based on hysteresis effects. We have performed some selected simulations on a larger system size; 40×80 nodes. Comparisons between the results of the two system sizes are found in Figure 7. The first order transition in (b) persists also for the larger system. If the signs of first order had been weaker for larger system sizes, then finite size effects had been the cause for apparent first order transitions. However, this is not the case here. Future work with more detailed and comprehensive investigations are needed to answer this question about the order with certainty.

The noisy character of the vertical parts, showing continuous transitions, can be attributed to the geometrical heterogeneity of the system. Some parts of the system are more active in transportation than others. In such rather small systems self-averaging is small and by chance the minority phase is to a larger or smaller extent placed in inactive parts of the system. This gives a shift in position

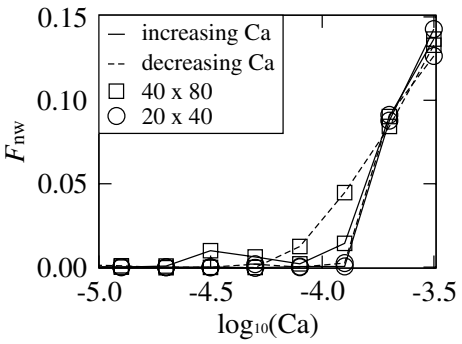

(a) $M = 1$

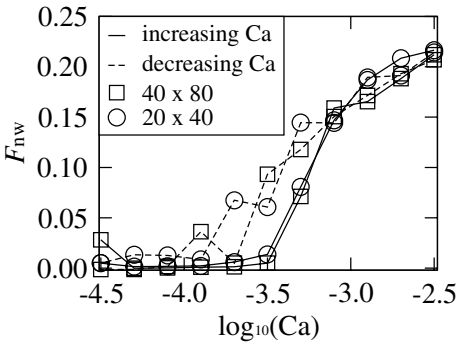

(b) $M = 10$

Fig. 7. Two samples of simulations on two different system sizes. The saturation is $S_{nw} = 0.3$ in both cases. The value of M is the only difference between (a) and (b). The transitions are (a) continuous or weakly first order, and (b) first order. The important aspect is that the hysteresis effects do not get smaller with increasing system size.

of the transition, i.e. noise, but does not affect the correlation between minority phase bubbles that are placed in active regions of the system. In fact these bubbles that are only held back by capillary forces are all correlated upon onset of mobilization. The motion of one bubble in one place relieves the pressure on all other minority bubbles in the system. The opposite is also true, when this bubble stops again, the pressure on the others increase immediately and this is likely to cause the onset of mobilization elsewhere. This is consistent with having infinite correlation length in statistical mechanics at continuous transitions.

The sloped sections of the boundaries, which from the hysteresis loop consideration show signs of first order transitions, show different characteristics. The viscosity ratio is unfavorable and the mobilization requires more pressure on a bubble, but when mobilized, larger bubbles or connected bubbles are involved. However, this effect is more local in the sense that the minority phase is not moving a little bit here and a little bit there in the form of different bubbles, but rather one larger region moves for a longer time when it is first mobilized. This correspond to a non-infinite correlation length.

6 Conclusion

This study concerns steady-state properties of two-phase flow in porous media. Average flow properties are monitored by using a network simulator on pore level. A systematic change of the system parameters: phase saturation, viscosity ratio, and capillary number, is performed. We demonstrate how the system can be in either one of three dynamical states or phases. These are: single-phase wetting flow, two-phase flow, and single-phase nonwetting flow. Upon passing from one dynamical phase to another the system undergoes a dynamical phase transition. The phase diagram for the dynamical phases is revealed and its properties are discussed.

By means of hysteresis we estimate the order of the phase transitions and we find that both continuous and first order transitions occur across different parts of the phase-boundaries. This is connected to two very different situations. One situation is when the viscosity ratio is defined to be favorable with respect to the majority phase: both capillary forces and viscous forces hold back the minority phase from flowing, next to this transition. The other case is when the viscosity ratio is defined to be unfavorable: only capillary forces try to hold back the minority phase next to the transition.

The phase diagram that is provided is for steady-state properties. This should be set in perspective to the phase diagrams by Lenormand et al. for drainage invasion flow properties [4,5]. Although the fact that the system investigated is a particular steady-state two-phase flow system, we argue that the general structure of the dynamical phase diagram has a universally valid structure.

We find that the definition of the capillary number is of major importance. Whereas for the actual two-phase flow region we employ a volume averaged viscosity in the definition, it turns out that the actual locations of the phase boundaries are determined by the capillary number based on the viscosity of the single phase in question. Based on the relationships between the capillary numbers (theoretical part) and limiting locations of the phase boundaries (found by the simulations) we establish a semi-empirical theory for the location of the phase boundaries. Upon direct comparison this theory is found to be in agreement with the simulated data points.

H.A.K. thanks VISTA, a collaboration between Statoil and the Norwegian Academy of Science and Letters, for financial support. We thank E. Skjetne for very valuable discussions, in particular in connection with Section 4 where his contribution was substantial.

References

1. F.A.L. Dullien. *Porous Media: Fluid Transport and Pore Structure* (Academic Press, San Diego, 1992)
2. M. Sahimi, *Flow and Transport in Porous Media and Fractured Rock* (VCH Verlagsgesellschaft mbH, Weinheim, 1995)

3. D. Tiab, E.C. Donaldson, *Petrophysics* (Gulf Publishing Company, Houston, 1996)
4. R. Lenormand, C. Zarcone, A. Sarr, J. Fluid Mech. **135**, 337 (1983)
5. R. Lenormand, E. Touboul, C. Zarcone, J. Fluid Mech. **189**, 165 (1988)
6. D.G. Avraam, A.C. Payatakes, J. Fluid Mech. **293**, 207 (1995)
7. D.G. Avraam, A.C. Payatakes, Transport in Porous Media **20**, 135 (1995)
8. D.G. Avraam, A.C. Payatakes, Ind. Eng. Chem. Res. **38**, 778 (1999)
9. E.W. Washburn, Phys. Rev. **17**, 273 (1921)
10. J. Koplik, T.J. Lasseter, Soc. Pet. Eng. J. **25**, 89 (1985)
11. G.N. Constantinides, A.C. Payatakes, J. Colloid Interface Sci. **141**, 486 (1991)
12. G.N. Constantinides, A.C. Payatakes, AIChE Journal **42**, 369 (1996)
13. D.H. Rothman, J. Geophys. Res. **95**, 8663 (1990)
14. B. Ferreol, D.H. Rothman, Transport in Porous Media **20**, 3 (1995)
15. K. Langaas, P. Papatzacos, Transport in Porous Media **45**, 241 (2001)
16. E. Aker, K.J. Måløy, A. Hansen, G.G. Batrouni, Transport in Porous Media **32**, 163 (1998)
17. E. Aker, K.J. Måløy, A. Hansen, Phys. Rev. E **58**, 2217 (1998)
18. H.A. Knudsen, E. Aker, A. Hansen, Transport in Porous Media **47**, 99 (2002)
19. P.M. Gerhart, R.J. Gross, J.I. Hochstein, *Fundamentals of fluid mechanics*, 2nd edn. (Addison Wesley, 1992)
20. S. Roux, unpublished
21. H.A. Knudsen, A. Hansen, Phys. Rev. E **65**, 056310 (2002)